Quantitative AES and XPS: Tests of Theory Using AES and XPS Databases with REELS Background Subtraction

M. P. Seah, I. S. Gilmore and S. J. Spencer

Centre for Optical and Analytical Measurement, National Physical Laboratory, Teddington, Middlesex TW11 0LW, UK
(email: martin.seah@npl.co.uk)

(Received December 12, 2001; accepted February 6, 2002)

For quantitative analysis by AES and XPS, it is important to test the theory and to use the correct sensitivity factors. We develop our previous analyses of peak area intensities for elemental spectra in digital Auger and X-ray photoelectron databases measured using a fully calibrated spectrometer. The intensities, instead of being analysed after removal of a Tougaard background are now analysed after removal of the extrinsic characteristic loss background by deconvolving the elemental angle-averaged reflected electron energy loss spectrum (REELS). The photoelectron spectra now show clear intrinsic shake-up intensities, reduced to around 30% of the total peak intensities. A comparison of theory and experiment within a new matrix-less quantification formulation, using average matrix sensitivity factors, leads to correlations with rms scatters of 8% and 11% for AES and XPS, respectively, for a very wide range of transitions. This gives formulae and values of sensitivity factors, appropriate for use with spectrometers calibrated to give true spectra.

1. Introduction

Quantitative analysis of surfaces by Auger electron spectroscopy (AES) and X-ray photoelectron spectroscopy (XPS) is important in many industrial sectors [1]. Very rarely has there been any attempt to correlate measurements between AES and XPS although this is both useful and important. We have developed, at NPL, elemental digital databases for homogeneous materials using AES and XPS to test and validate the theoretical calculation of intensities. Thus, we develop a secure foundation for quantitative analysis using simple, practical equations with a relative sensitivity factor based approach.

There have been many excellent compilations of databases of spectra for AES and XPS listed in references [2] and [3], however, in those compilations, the electron spectrometers had unknown intensity/energy response functions. For both AES [4] and XPS [5], individual instrument response functions may vary, one from another, such that intensity ratios for different elements may differ by up to an order of magnitude. We have, therefore, developed methods [6,7] for calibrating the intensity/energy response functions for both AES and XPS instruments to remove this problem and to generate traceable databases.

In our earlier studies, we have presented the experimental data for AES [2,8,9] and XPS [3,8]. These measurements are then compared with the theory [3,9] to show how the correct parameters [3,9-11], cross-sections [3,10] etc., can be chosen in order to obtain a good correlation. Although the correlations were good, with no independent fittings or normalisations, there were significant divergencies for particular elements. For both AES [9] and XPS [3], these divergencies were correlated and were thought to arise from a failure of the applicability of the Universal Tougaard background subtraction method [12], as it was used in those studies to remove the extrinsic energy loss intensity when applied to a wide range of separate pure elements. It should be stressed that the use of the Tougaard Universal cross section is still valid if one is considering the normal analytical situation of the relative intensities of two peaks from a single spectrum [11], but can lead to significant error when comparing intensities from different materials.

We replace Tougaard's method for the removal of the background for the inelastically scattered Auger or X-ray photoelectrons by a method involving deconvolution using an angle-averaged REELS database [13]. The angle averaging is important and has not been previously

included in such approaches. This method does not account for the double sampling of the surface and so we expect the angle-averaged REELS method to over-remove the surface plasmons and under-remove the bulk plasmons. It is expected that these two effects will approximately balance each other in the overall intensity analysis [14].

2. Experimental Conditions

The experimental conditions for acquiring the AES and XPS data are given in references [2] and [3], respectively. Briefly, all of the data provided here were recorded using the *Metrology Spectrometer II*. The spectra were corrected for the detector dead time [15] with an accuracy better than 1%, and also for the spectrometer intensity/energy response function [6]. AES data were acquired for 5 keV and 10 keV beam energies with the electron beam at 30° to the surface normal and the detected electrons at 16° to the surface normal. Similarly, for XPS, unmonochromated Al and Mg X-ray sources were used with an angle of incidence of 51° and an angle of emission for the photoelectrons of 14°. These two angles are not in the same azimuth and so allow the angle between the incident X-rays and the detected electrons to be set at the magic angle of 54.7°. The REELS data [13] were acquired for an incident 1 keV electron beam at 35° to the surface normal with the detected electrons at 15° from the surface normal. This gave an average scattering angle of 142°. All spectra were recorded in the constant ΔE mode for pure elemental samples, sputtered clean with argon ions. Figure 1 shows the elements studied in the AES database.

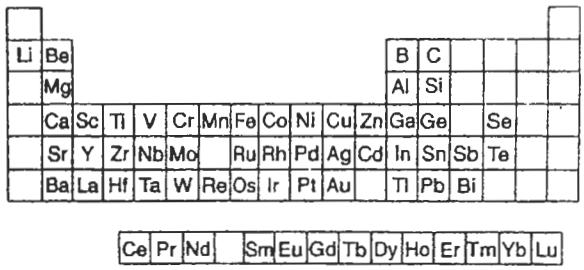

Fig 1 Elements in the AES database recorded using the *Metrology Spectrometer II*.

3. Theoretical Parameters for the Intensities

3. (a) Auger electron spectroscopy

The Auger electron intensity for an element A, for the sum of all of the transitions involving ionisations with the same initial core level principal quantum number, is given by [9]

$$I_A^{\infty}(\text{theor},CK,E_o) = \gamma_{AX}\ \sec\alpha\ N_A Q_A(E_{AX}) \cos\theta \sum_i n_{AX_i}\ \sigma_{AX_i}(E_o) \times [1+r_A(E^B_{AX_i}, E_o, \alpha)]\ \lambda_A(E_{AX}) \quad (1)$$

where γ_{AX} is the probability that the ionised core level X in element A is filled with the ejection of an Auger electron [16,17], $\sigma_{AX}(E_o)$ is the ionisation cross section [18] of the core level X in the element A for electrons of energy E_o, n_{AX} is the population of the level X, α is the angle of incidence of the excitation beam from the surface normal, $r_A(E^B_{AX_i}, E_o, \alpha)$ is the additional ionisation of the core level X with binding energy $E^B_{AX_i}$ arising from backscattered energetic electrons [19], $Q_A(E_{AXYZ})$ is a term allowing for the reduction in overall escape probability of electrons from the solid arising from elastic scattering [20,21], N_A is the atomic density of the A atoms, $\lambda_A(E_{AX})$ is the inelastic mean free path (IMFP) [22] for the Auger electrons with average energy E_{AX} in the sample A, and θ is the angle of emission of the detected electrons from the surface normal.

In Eqn (1), we have summed all of the Auger electron intensity arising from ionisations in one shell since Coster Kronig transitions change the relative intensities of the Auger electrons generated by the filling of the different ionised subshells. Thus, calculating the intensities of individual Auger electron peaks is difficult, whereas calculating the total Auger electron intensity from a given shell is straightforward. Experimentally, it is difficult to separate the relevant peak areas accurately and so Eqn (1) also provides the practical intensity to measure.

3. (b) X-ray photoelectron spectroscopy

The X-ray photoelectron intensity for an element A for a detector at the magic angle is given by [3]

$$I^{\infty}_{AX_i}(\text{theor},h\nu) = n_{AX_i}\sigma_{AX_i}(h\nu)\ \sec\alpha\ N_A\, Q_A(E_{AX_i})\, \lambda_A(E_{AX_i}) \quad (2)$$

where n_{AX_i} is the population of electrons in the subshell i of the core level shell X of element A and $\sigma_{AX_i}(h\nu)$ is the ionisation cross section [23] for the relevant core level for photons of energy hν. Equation (2) does not include a term for the

asymmetry parameter since the elastic scattering reduces this to a modified asymmetry parameter which has zero contribution (i.e. adds a factor of unity into Eqn (2)) at the magic angle [20].

4. SUMMARY OF THE PREVIOUS CORRELATIONS

Our previous analysis of the spectral data is straightforward but involves a number of steps which it is worth summarising here so that any changes in those steps are clear. In the analysis of the AES data, first we correct for the effects of surface roughness, next we remove the inelastically scattered primary electron background [2,24], then a background using the Tougaard Universal cross section with parameters B and C set at 3006 eV^2 and 1643 eV^2, and finally a Sickafus background [25]. This removed all of the backgrounds in AES so that the peak areas could be determined and their ratio to that calculated from Eqn (1) evaluated.

This analysis gave a good correlation with theory for K, L, M and N shell ionisations, and showed that Casnati *et al*'s [18] cross section was better than Gryzinski's [26]. However, certain systematic divergencies dependent on Z remained.

The analysis for XPS was very similar to that for AES. First, the X-ray satellites were removed [3], then a Tougaard background using the Universal cross section.

This analysis gave a good correlation with theory for all transitions and showed that Scofield's cross sections [23] were better than those of Yeh and Lindau [27]. However, the systematic divergencies dependent on Z, noted above for AES, also remained. It was considered that these correlated systematic errors would be reduced if the Tougaard background subtraction method was replaced by the method involving the angle-averaged REELS data [13] which are unique for each element.

5. RESULTS OF THE INTENSITY ANALYSIS

Details of the REELS background removal are given elsewhere [28]. Figure 2(a) shows the Al photoelectron spectra for the 2s and 2p peaks after satellite subtraction (S); the spectrum after removal of a Tougaard background (T) and after removal of the angle-averaged REELS background (R). The REELS approach removes significantly more of the background than the

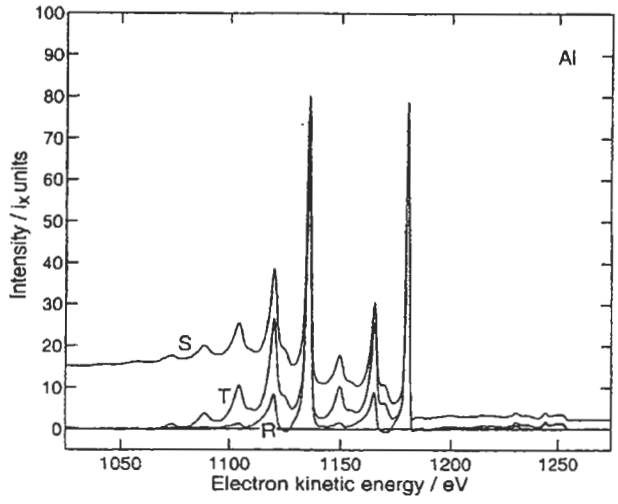

(a)

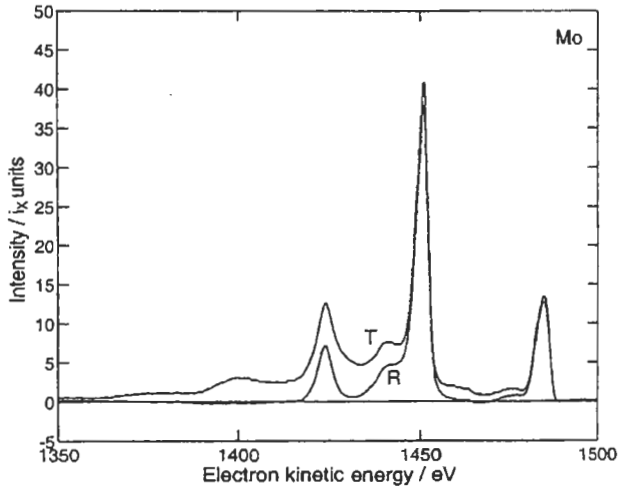

(b)

Fig 2 (a) Al XPS data using Mg X-rays: S = true spectrum after satellite subtraction, T = background subtracted using the Tougaard Universal cross section (B = 3006 eV^2, C = 1643 eV^2), R = background subtracted using angle-averaged REELS data [13], (b) Mo data using Al X-rays.

Tougaard method when used with the values of B and C selected earlier. The surface plasmon is subtracted a little too strongly, as expected, but the remaining bulk plasmon is at about the intensity calculated for intrinsic plasmons. Figure 2(b) shows the results for the 4s, 4p and 4d peaks for Mo. Analysis of a selected group of elements for the areas in the peak (P) and the remaining background (B) using the Tougaard and REELS methods is given in Table 1.

In general, the intrinsic background after the Tougaard method gives a B/P ratio of 1.15, such

Table 1 Intrinsic area, B, and the peak area, P, as a percentage of the total area B+P after Tougaard and angle-averaged REELS background subtraction

Element	Tougaard			REELS		
	P %	B %	B/P	P %	B %	B/P
Al	36	64	1.78	73	27	0.37
Cu	56	44	0.79	76	24	0.32
Mo	47	53	1.13	88	12	0.14
Sn	51	49	0.96	80	20	0.25
Ta	48	52	1.08	72	28	0.39
mean	48	52	1.15	78	22	0.29

that the intrinsic background area, B, is larger than the peak area, P, whereas, after angle-averaged REELS deconvolution, the average value of B/P is 0.29. For a given peak area, the Tougaard intrinsic background area is thus approximately 4 times the angle-averaged REELS intrinsic background area and appears to be excessive.

From the data of Steiner *et al* [29], we may calculate the fraction of the intensity arising as a result of intrinsic losses. For Be, Na, Mg and Al this fraction is 31%, 41%, 24% and 10%, respectively. These results are consistent with Penn's [30] calculations and average 27%. This gives B = 0.27 and a B/P ratio of 0.37 which is of the same order as the average value of 0.29 given in Table 1 for the angle-averaged REELS background subtraction, but one third of the value found using the Tougaard Universal cross section with B = 3006 eV^2 and C = 1643 eV^2.

Using the angle-averaged REELS data for background subtraction in place of the Tougaard Universal cross section we obtain, in Figs 3 and 4, the new results for the experimental peak area intensities for AES and XPS.

The ratios of experiment to theory for each element are now improved compared with our earlier analysis. The scatter factors of the AES results for this ratio are ×/+ 1.28 for the data above 180 eV. [Note that a factor of 1.28 is 2.5 times the diameter of the plotted circles in Fig 3]. The XPS results give scatter factors of ×/+ 1.21 for both Mg and Al X-rays, if we exclude the very weak s level peaks for Z > 20 and the valence band peaks with binding energies of less than 17 eV.

A clear correlation exists for the remaining divergence between theory and experiment that

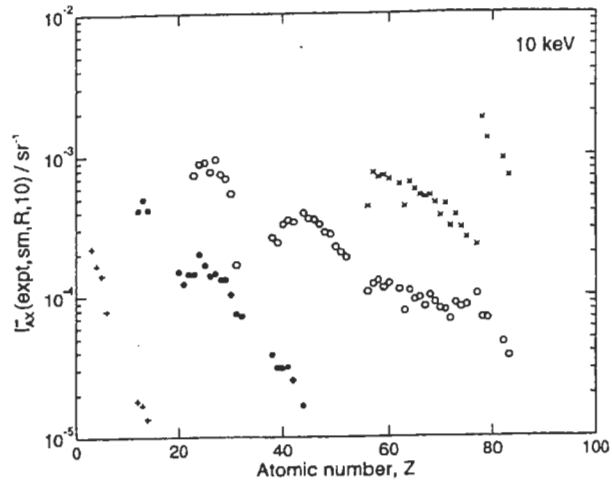

Fig 3 Experimental peak areas for the K shell (+), L shell (*), M shell (o) and N shell (x) electrons in AES using angle-averaged REELS background subtraction, I^{∞}_{AX} (expt,sm,R,E_o) for 10 keV incident beam energy.

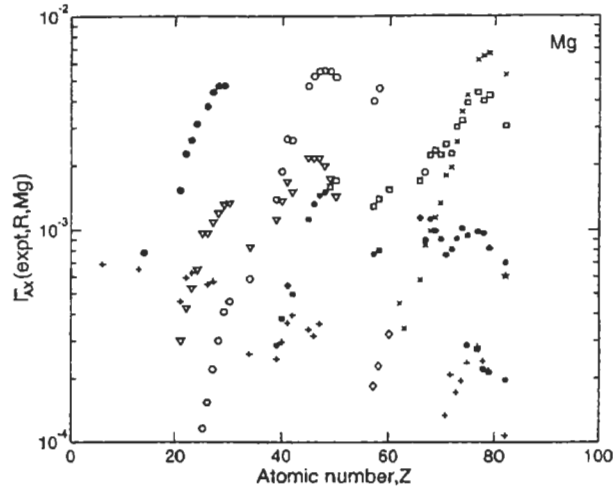

Fig 4 Experimental peak areas for the 1s (+), 2p (●), 3p (▽), 3d (o), 4p (*), 4d (□), 4f (x), 5p (◊) and 5d (☆) electrons in XPS using angle-averaged REELS background subtraction, I^{∞}_{A} (expt,R,hv) for unmonochromated Mg X-rays.

exists for AES and XPS. This shows that there is still an element-specific error. If we assume that there is a single correction factor, G, for the experimental peak areas given by the average of the AES and XPS errors for each element, we may re-determine the scatters. The G values are given in reference [28]. The scatter of the ratio of experiment to theory for AES now falls from ×/+ 1.28 to ×/+ 1.09 for the 10 keV data for peaks above 180 eV. The total scatters in XPS for the

Mg and Al X-ray data fall, respectively, from ×/÷ 1.21 and ×/÷ 1.21 to ×/÷ 1.12 and ×/÷ 1.11 for the data excluding both the s levels for Z > 20 and also those peaks for binding energies < 17 eV.

The element-specific correction factor G, may arise from inadequacy, either in the angle-averaged REELS background removal used to obtain the experimental peak area, or in the material-to-material dependence of the TPP-2M equation used in calculating the theoretical values of the intensities, or in some combination of both topics. Fortunately, these problems can be circumvented as described below.

As noted in previous work [3,9], the experimental intensities that are measured are elemental relative sensitivity factors. These are not the correct factors for the quantitative analysis of homogeneous mixtures using the usual simple equation with relative sensitivity factors with no matrix factors. That equation may be written:

$$X_A = \frac{I_{Am} / I_A^{Av}}{\sum_i I_{im} / I_i^{Av}} \qquad (3)$$

where X_A is the atomic fraction of A, I_{im} is the Auger or X-ray photoelectron intensity for element i in the matrix m and I_i^{Av} is a sensitivity factor for element i in AES or XPS, based on an average matrix. Very often, Eqn (3) is erroneously written with the pure element sensitivity factors, instead of the sensitivity factors based on an average matrix. In that case, matrix factors are needed which have values, for AES, in the range 0.1 to 7 and for XPS, in the range 0.3 to 3, which should then be included in Eqn (3), as discussed elsewhere [3,9].

The average matrix sensitivity factors may be calculated for AES by

$$I_A^{Av}(\text{theor,CK},E_o) = \gamma_{AX} \sec\alpha \; N_{Av} \; Q_{Av}(E_{AX}) \sum_i n_{AX_i} \sigma_{AX_i}(E_o) \times [1 + r_{Av}(E^B_{AX_i}, E_o, \alpha)] \lambda_{Av}(E_{AX_i}) \qquad (4)$$

and for XPS by

$$I_A^{Av}(\text{theor},h\nu) = n_{AX_i} \sigma_{AX_i}(h\nu) N_{Av} Q_{Av}(E_{AX_i}) \lambda_{Av}(E_{AX_i}) \qquad (5)$$

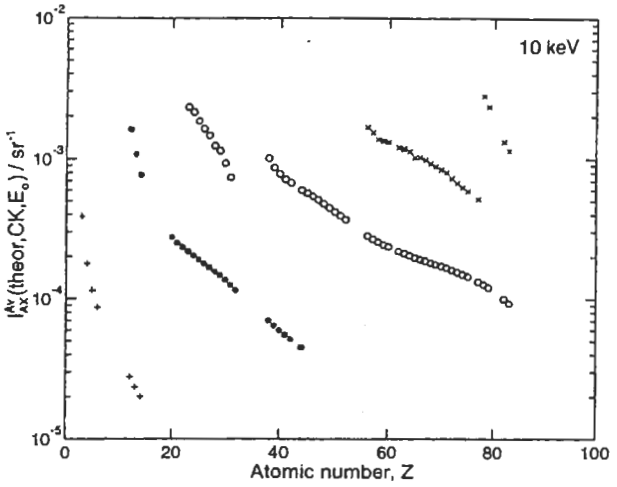

Fig 5 Calculated Auger electron average matrix sensitivity factors, I^{Av}_{AX}(theor,CK,E_o), for K shell (+), L shell (*), M shell (o) and N shell (x) for elements in an average matrix for 10 keV electrons incident at 30° to the surface normal [×/÷ 1.09], for peaks with kinetic energies above 180 eV.

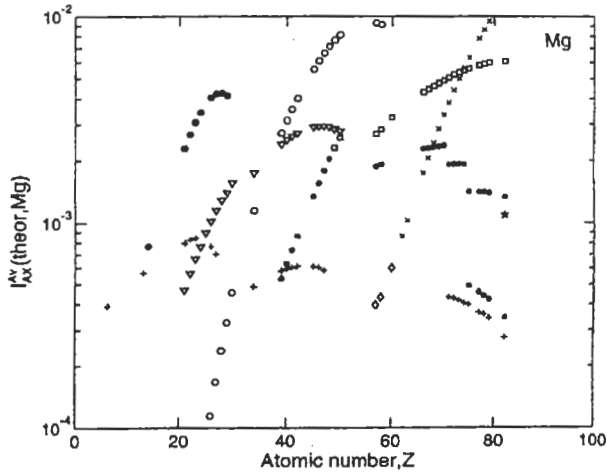

Fig 6 Calculated X-ray average matrix sensitivity factors, I^{Av}_{AX}(theor,hν), for the 1s (+), 2p (●), 3p (▽), 3d (o), 4p (*), 4d (□), 4f (x), 5p (◊) and 5d (☆) electrons in XPS for elements in an average matrix for incident Mg X-rays at the magic angle.

where the equations to calculate the parameters N_{Av}, Q_{Av} and λ_{Av} for the average matrix, subscripted "Av", are given in references [3] and [9]. All of the parameters in Eqns (4) and (5) are smoothly varying with atomic number, Z, as shown in Figs 5 and 6.

In this approach, the two possible sources of error cited earlier disappear. The element-to-element dependence of the IMFP no longer appears as all of the data are for the average matrix. The uncertainties of the REELS

background subtraction are also unimportant since the quantification is applied to a single spectrum where errors scale all of the peak intensities equally. Equation (3) is accurate and simple and, unlike the traditional approach needing matrix factors, it is not necessary to know the composition of the sample in order to quantify it!

6. CONCLUSIONS

The absolute intensities of the peaks from homogeneous materials, when using the Tougaard Universal cross section for background subtraction, may be in error by up to a factor of two. By deconvolving AES and XPS spectral data using angle-averaged REELS data, more accurate absolute intensities are obtained. The remaining correlated errors between the AES and XPS results for the ratio of experiment to theory indicate that a further, Z-dependent correction factor exists. This factor is attributed to errors either in the angle-averaged REELS method or in the material-to-material dependence of the IMFP. These errors may be removed by quantifying spectra in AES and XPS, using a simple matrixless equation, Eqn (3), where the sensitivity factors are those of the average matrix. The average matrix sensitivity factors then correlate with the theoretical predictions with scatter factors of ×/+ 1.08 and 1.09 for the 5 keV and 10 keV AES data, respectively (peak energies > 180 eV), and ×/+ 1.12 and 1.11 for the Mg and Al X-ray data, respectively (excludes s peaks for $Z > 20$ and levels with BE < 17 eV). These final scatters are excellent and indicate that calculated average matrix sensitivity factors, using the parameters given, should provide quantification at least at this level of accuracy and probably better.

REFERENCES

[1] M. P. Seah and D. Briggs, in Practical Surface Analysis, Vol.1 - Auger and X-ray Phtotoelectron Spectroscopy, Eds., D Briggs and M P Seah, Wiley, Chichester (1990) p 1-18.

[2] M. P. Seah and I. S. Gilmore, J. Vac. Sci. Technol. A **14**, 1401 (1996).

[3] M. P. Seah, I. S. Gilmore, and S. J. Spencer, J. Electron Spectrosc. **120**, 93 (2001).

[4] M. P. Seah and G. C. Smith, Surf. Interface Anal. **17**, 855 (1991).

[5] M. P. Seah, Surf. Interface Anal. **20**, 243 (1993).

[6] M. P. Seah, J. Electron Spectrosc. **71**, 191 (1995).

[7] NPL Auger Electron Spectrometer Intensity Calibration Software, A.1; NPL X-ray Photoelectron Spectrometer Intensity Calibration Software, X.1; http://www.npl.co.uk/npl/cmmt/sis/index.html.

[8] M. P. Seah, J. Electron Spectrosc. **100**, 55 (1999).

[9] M. P. Seah and I. S. Gilmore, Surf. Interface Anal. **26**, 908 (1998).

[10] M. P. Seah and I. S. Gilmore, Surf. Interface Anal. **26**, 815 (1998).

[11] M. P. Seah, Surf. Sci. **420**, 285 (1999).

[12] S. Tougaard, Surf. Interface Anal. **11**, 453 (1998).

[13] M. P. Seah, Surface Sci. **471**, 185 (2001).

[14] A. Cohen Simonsen, F. Yubero, and S. Tougaard, Surf. Sci. **436**, 149 (1999).

[15] M. P. Seah, Surf. Interface Anal. **23**, 729 (1995).

[16] E. H. S. Burhop, The Auger Effect and Other Radiationless Transitions, Cambridge, The University Press (1952).

[17] J. I. Goldstein and H. Yakowitz (Eds), Practical Scanning Electron Microscope, Plenum Press, New York (1975) p 88.

[18] E. Casnati, A. Tartari, and C. Baraldi, J. Phys. B **15**, 155 (1982).

[19] R. Shimizu, Jpn. J. Appl. Phys. **22**, 1631 (1983).

[20] A. Jablonski, Surf. Interface Anal. **23**, 29 (1995).

[21] M. P. Seah and I. S. Gilmore, Surf. Interface Anal. **31**, 835 (2001).

[22] S. Tanuma, C. J. Powell, and D. R. Penn, Surf. Interface Anal. **21**, 165 (1994).

[23] J. H. Scofield, J. Electron Spectrosc. **8**, 129 (1976).

[24] D. Jousset and J. P. Langeron, J. Vac. Sci. Technol. A **5**, 989 (1987).

[25] E. N. Sickafus, Phys. Rev. B **16** 1436 (1977).

[26] M. Gryzinski, Phys. Rev. **138A**, 336 (1965).

[27] J. J. Yeh and I. Lindau, Atomic Data and Nuclear Data Tables **32**, 1 (1985).

[28] M. P. Seah, I. S. Gilmore, and S. J. Spencer, Surf. Interface Anal. **31**, 778 (2001).

[29] P. Steiner, H. Höchst, and S. Hüfner, Z. Phys. B **30**, 129 (1978).

[30] D. R. Penn, Phys. Rev. Lett. **38**, 129 (1977).